Steel and Composite Structures, *Vol. 33, No. 6* (*2019*) *837-847*
DOI: https://doi.org/10.12989/scs.2019.33.6.837

Energy absorption investigation of square CFRP honeycomb reinforced by PMI foam fillers under quasi-static compressive load

Hao Zhou, Rui Guo*, Kuo Bao, Haiyang Wei and Rongzhong Liu

School of Mechanical Engineering, *Nanjing University of Science and Technology*, *200 Xiaolingwei Street*, *Nanjing 210094*, *P. R. China*

(*Received August 24, 2019, Revised November 17, 2019, Accepted November 26, 2019*)

Abstract. A type of hybrid core made up of thin-walled square carbon fiber reinforced polymer (CFRP) honeycomb and Polymethacrylimide (PMI) foam fillers was proposed and prepared. Numerical model of the core under quasi static compression was established and validated by corresponding experimental results. The compressive properties of the core with different configurations were analyzed through numerical simulations. The effect of the geometrical parameters and foam fillers on the compressive response and energy absorption of the core were analyzed. The results show that the PMI foam fillers can significantly improve the compressive strength and energy absorption capacity of the square CFRP honeycomb. The geometrical parameters have marked effects on the compressive properties of the core. The research can give a reference for the application of PMI foam materials in energy absorbing structures and guide the design and optimization of lightweight and energy efficient cores of sandwiches.

Keywords: CFRP; honeycomb; PMI foam filler; quasi static; compressive property; numerical simulation

1. Introduction

Sandwich structures, which are made of two rigid face sheets and a soft core, are playing an important role in protection structures in different areas. As the main energy absorbing part in a sandwich structure, the properties of the core have significant effects on the protective performance of the structure. In recent years, the topological optimization of cores to reduce the weight, and at the mean time to increase the energy absorbing capacity of sandwich structures, has always been the research focus in relevant areas (Taghipoor and Noori 2018a, b, and c).

Recently, fiber reinforced composite materials have gain lots of concerns due to its advantages in mechanical properties, including low density, high specific strength and stiffness, strong corruption resisting properties and enduring performances, as well as outstanding designable ability. Research on the application of fiber reinforced composite materials in sandwich cores have been conducted by many researchers. Russell *et al.* (2008) fabricated carbon fiber epoxy matrix composite honeycombs with various fiber architectures and measured their out-of-plane compressive and in-plane shear responses as a function of relative density. Theoretical predictions of the compressive and shear strength were also carried out and the research provided new opportunities for lightweight, high strength structural design. Hu *et al.* (2016) designed and fabricated a novel carbon fiber reinforced composite lattice truss sandwich panel through mould pressing method, the strength and failure modes of this novel structure were analyzed by compressive and shear tests. Norouzi and Rostamiyan (2015) improved the mechanical strength peak of fiber/epoxy sandwich panels with new lattice cores. The flatwise compression behavior of this novel panels were analyzed by experiments and numerical simulations. Fan *et al.* (2006) proposed stretching dominated lattice materials reinforced by carbon fiber and studied the mechanical behaviors by experiments and predictions. The results showed that the carbon fiber reinforced lattice materials are much stiffer and stronger than foams and honeycomb.

For lightweight and energy efficient design, thin-walled composite structures with low-density fillers, including both metallic and polymeric foams, have drawn increasing interest (Aydin and Gundogdu 2018). Reddy and Wall (1988) analyzed the effect of low density polyurethane (PU) foam on the axial crushing of thin-walled circular tubes and found that the filler can improve the energy absorption property of the tubes. Mozafari *et al.* (2015) investigated the effect of PU foam fillers on the in-plane lateral crushing properties of honeycomb cores, which showed that the foam fillers significantly increased the core strength and improved the energy absorption capacity. Liu *et al.* (2017) and Zhang *et al.* (2019) experimentally studied the effect of Expanded Polypropylene (EPP) foam fillers on the mechanical properties of aluminum honeycomb panels under both quasi-static and dynamic compressive loadings. George *et al*. (2014) fabricated CFRP sandwich panels with hybrid foam filled CFRP pyramidal lattice cores and analyzed their mechanical response. The novel sandwich structures compare favorably with other lightweight energy absorbing materials and structures. Hussein *et al*. (2017) experimentally investigated the axial crushing behavior of square aluminium tubes with different configurations, such

*Corresponding author, Ph.D.,
E-mail: guorui@njust.edu.cn

http://www.techno-press.org/?journal=scs&subpage=6 ISSN: 1229-9367 (Print), 1598-6233 (Online)

as hollow tubes, alumimium honeycomb-filled tubes, PU foam-filled tubes and tubes filled with both PU foam and aluminium honeycomb. The results show that the fillers can significantly improve the energy absorption capacities of the tubes.

PMI foams have a crosslinked, 100% closed cellular structure and the uniform material distribution throughout the cell walls gives excellent structural stability and a high level of mechanical strength, which offers the largest potential for manufacturing lightweight sandwich structures with foam core (Seibert 2000). However, there is limited research on PMI foam filled composite honeycomb cores, which can help us to understand their advantages in mechanical properties and energy absorbing capacities.

In summary, effects of PMI foam fillers on the mechanical properties and energy absorption capacity of the composite honeycomb cores still remain unclear. In order to find out the advantages of CFRP honeycomb reinforced by PMI foam fillers in energy absorption properties under quasi static compressive load, we proposed a hybrid core constructed by thin-walled square CFRP honeycomb with PMI foam fillers. The core was prepared and quasi static compression tests were carried out for the validation of the numerical model. Numerical simulations were conducted to analyze the effect of the geometric parameters and foam fillers on the quasi static compressive properties of the hybrid bore, which can provide some new ideas for novel sandwich core configurations and guide the lightweight and energy efficient design of novel sandwich core structures.

2. Preparation and quasi static compression test

A hybrid core structure made from square CFRP honeycomb and PMI foam fillers was proposed and prepared. Firstly, the CFRP sheets based on SKO® woven carbon fiber cloth with areal density of 200 g/m^2 and low-viscosity EP51 epoxy resin was prepared via resin transfer moulding method and the mechanical properties were measured through quasi static compression and tensile tests in both 0/90° and 45° fiber directions. The mechanical properties of the woven CFRP material used in this paper are shown in Table 1.

Three types of PMI foams with different densities (notated as 52-X, 75-X and 110-X, respectively) were investigated in this paper. Quasi static compressive

Table 1 Mechanical properties of woven CFRP material

Notation	Property	Value
E_0	0/90° tensile modulus	4.8 GPa
E_{45}	45° tensile modulus	6.0 GPa
σ_0^t	0° tensile strength	195 MPa
σ_0^c	0° compressive strength	191 MPa
σ_{45}^t	45° tensile strength	103 MPa
σ_{45}^c	45° compressive strength	153 MPa
υ	Poisson's ratio	0.16
ρ_h	Density	1450 kg/m^3

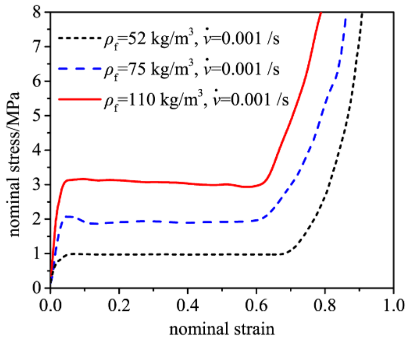

Fig. 1 Quasi static compression results of PMI foams with different dehpgnsities

Table 2 Mechanical properties of PMI foam with different densities

Properties	52-X	75-X	110-X
Density (kg/m^3)	52	75	110
Compressive modulus (MPa)	47	71	119
Compressive strength (MPa)	0.99	2.0	3.0
Tensile modulus (MPa)	74	120	200
Tensile strength (MPa)	1.7	2.6	4.1
Shear modulus (MPa)	23	30	70
Shear strength (MPa)	0.92	1.6	2.7

properties from compression tests of different foams were shown in Fig. 1. Detailed mechanical properties of PMI foam with different densities are shown in Table 2.

As shown in Fig. 2, the preparation process of the CFRP honeycomb with PMI foam fillers is as follows:

(a) First the CFRP sheets with the thickness of t = 0.4 mm was cut into rectangular pieces as sketched in Fig. 2(a), with slots of width c = 0.4 mm, length $h_c/2$ and spacing l_w. The configuration of the core is controlled by the geometric parameters including the width of the CFRP pieces, h_c, and the spacing between honeycomb walls, l_w.

(b) Then the slotted rectangular pieces were assembled into the square honeycomb as shown in Fig. 2(b). The joints between honeycomb walls were adhesively bounded using a low viscosity epoxy adhesive.

(c) The PMI foam was cut into blocks with the dimension of length and width equal to l_w and height equals to h_c. Then the foam blocks with epoxy resin on their surfaces were inserted into the square honeycomb and lastly the assembled core was cured at 60°C for 2 hours. The prepared core structure with l_w = 10 mm and h_c = 20 mm is shown in Fig. 3.

According to the representative volume element of the core as shown in Fig. 4, the density of square CFRP honeycomb with PMI foam fillers, ρc, can be approximately given by

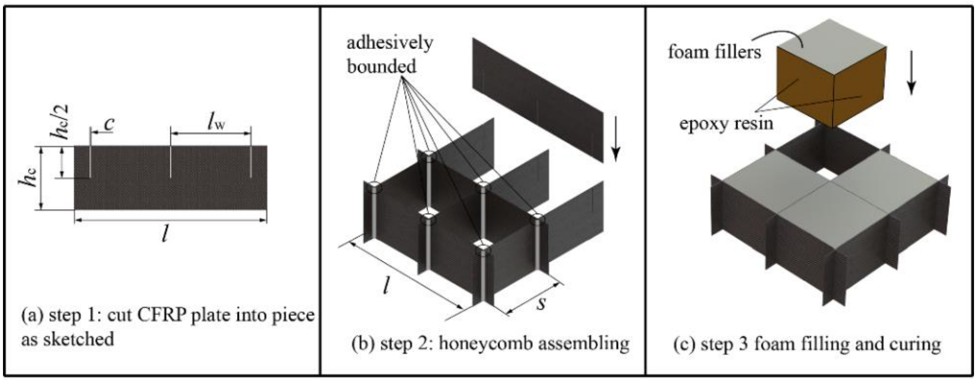

Fig. 2 Preparation process of CFRP honeycomb core with foam fillers

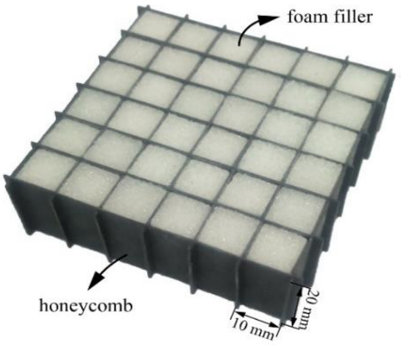

Fig. 3 Prepared CFRP core with PMI foam fillers (l_w = 10 mm, h_c = 20mm)

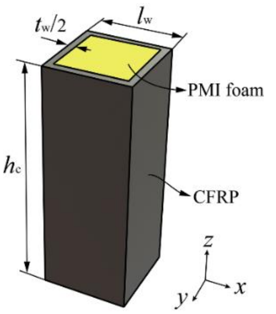

Fig. 4 Representative volume element of the core

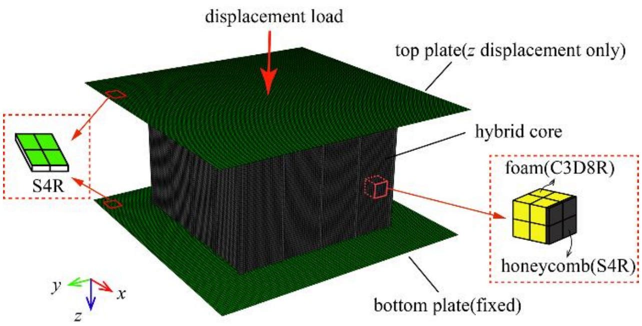

Fig. 5 Numerical model of CFRP honeycomb core with foam fillers under quasi static compression

$$\rho_c = \frac{2t_w}{l_w}\rho_h + \rho_f \tag{1}$$

where, ρ_h is the density of the CFRP materials and ρ_f is the density of the foam materials.

Then the quasi static compression tests were performed via the WAW-300B universal testing machine. In order to reduce the measuring error caused by frictions, two 3 mm-thick steel plates were adhesively bounded to the top and bottom surfaces of the core, respectively. High speed camera was applied to record the compression process of the CFRP honeycomb with foam fillers. The compressive force versus displacement data was output by the data recording computer.

3. Numerical modelling

3.1 Geometrical model and meshing

The quasi static compressive response of the CFRP honeycomb with foam fillers was analyzed by numerical simulations performed using the explicit time integration version of finite element code ABAQUS (version 2016). The numerical model is illustrated in Fig. 5.

The honeycomb was modelled using four-node shell elements notated as S4R while the PMI foam fillers were modelled by eight-node solid elements C3D8R. Cohesive contacts were applied at the interfaces of the honeycomb and foam fillers to describe the adhesive bounding. Rigid plates were set at the top surface and bottom surface of the core, respectively, and the core was tied to the rigid plates at the interfaces. The bottom plate was fixed while a uniform z-direction displacement was applied on the top plate to simulate the compressive load, of which the strain rate is 0.001 s-1.

Mesh sensitivity and effects of initial imperfection and boundary conditions were also discussed to guarantee the accuracy of the numerical model.

3.2 Modelling of CFRP materials

In the numerical model, the damage evolution is used in combination with Hashin’s damage initiation criterion for CFRP material. As sketched in Fig. 6, a single ply of

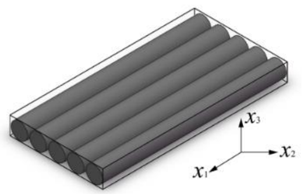

Fig. 6 Sketch illustrating the co-ordinate system for a single ply of a unidirectional laminate

a carbon fiber reinforced unidirectional lamina was considered, with the x_1 axis in the fiber direction, x_2 in the transverse direction and x_3 perpendicular to the plane of the ply. The unidirectional ply is transversely isotropic with respect to the fiber direction, i.e. x_1 axis. For a state of plane stress, the elastic response of the undamaged material is given by

$$\begin{pmatrix}\varepsilon_{11}\\ \varepsilon_{22}\\ \gamma_{12}\end{pmatrix}=\begin{pmatrix}\frac{1}{E_1} & \frac{-\nu_{12}}{E_1} & 0\\ \frac{-\nu_{21}}{E_2} & \frac{1}{E_2} & 0\\ 0 & 0 & \frac{1}{G}\end{pmatrix}\begin{pmatrix}\sigma_{11}\\ \sigma_{22}\\ \sigma_{12}\end{pmatrix} \tag{2}$$

where ε_{11} and ε_{22} are direct strains in the x_1 and x_2 direction, respectively, and γ_{12} is the engineering shear strain. The Young's moduli E_1 and E_2 in the x_1 and x_2 directions, along with the shear modulus G and Poisson's ratio ν_{21} are the four relevant elastic constants of the unidirectional lamina while ν_{21} is not an independent elastic constant and related to the other elastic constants via the relation $\nu_{21} = (E_2/E_1)\nu_{12}$.

As for the damage law, the lamina was taken to be linear elastic, as specified in Eq. (1), up to the initiation of damage. A nonlinear stress versus strain response accompanies damage progression due to a progressive drop in three moduli (E_1, E_2 and G) with increasing strain. Four scaler damage variables d_i are introduced, corresponding to four damage modes of the materials including tensile and compressive failure in the fiber and transverse directions, respectively. Detailed description of the damage law is given in the Appendix.

3.3 Modelling of PMI foam

The PMI foam fillers are modelled as crushable foam using hardening curves obtained by compression test on cubic foam samples. The compression process can be described as a linear elastic stage followed by a plastic hardening stage. Specifically in the plastic hardening stage, a phenomenological yield surface for a closed-cell foam was proposed by Deshpande and Fleck (2001), which is given by

$$F=\sqrt{q^2+\alpha^2\sigma_m^2}-\sigma_{\mathrm{yf}}\sqrt{1+\left(\frac{\alpha}{3}\right)^2}=0 \tag{3}$$

where σ_{yf} is the uniaxial tensile or compressive yield strength of the foam, q is the Von Mises stress, σ_{m} is the mean stress, α is a parameter defining the shape of the yield surface, which can be given by

$$\alpha=\frac{3k}{\sqrt{9-k^2}} \tag{4}$$

where $k=\frac{\sigma_{\mathrm{cf}}^0}{p_{\mathrm{cf}}^0}$, which is the ratios of the initial uniaxial yield stress σ_{cf}^0 to the hydrostatic compressive yield stress p_{cf}^0.

Based on the yield stress in hydrostatic compression, the evolution of the shape of the yield surface can be described as

$$p_{\mathrm{cf}}\left(\varepsilon_{\mathrm{vol}}^{\mathrm{pl}}\right)=\frac{\sigma_{\mathrm{cf}}\left(\varepsilon_{\mathrm{vol}}^{\mathrm{pl}}\right)\left[\sigma_{\mathrm{cf}}\left(\varepsilon_{\mathrm{axial}}^{\mathrm{pl}}\right)\left(\frac{1}{\alpha^2}+\frac{1}{9}\right)+\frac{p_{\mathrm{tf}}}{3}\right]}{p_{\mathrm{tf}}+\frac{\sigma_{\mathrm{cf}}\left(\varepsilon_{\mathrm{axial}}^{\mathrm{pl}}\right)}{3}} \tag{5}$$

where $\varepsilon_{\mathrm{vol}}^{\mathrm{pl}}$ is the plastic volumetric strain and p_{tf} is the hydrostatic tensile yield stress.

The stain rate effect of the foam material was also taken into account. A Cowper-Symonds overstress power law that defines strain rate dependence was specified, which has the form

$$\dot{\bar{\varepsilon}}^{\mathrm{pl}}=D(R-1)^n \tag{6}$$

where $\dot{\bar{\varepsilon}}^{\mathrm{pl}}$ is the equivalent plastic strain rate, D and n are material parameters that can be obtained by compression test of the material under different strain rates, and

$$R=\frac{\bar{\sigma}_{\mathrm{cf}}}{\sigma_{\mathrm{cf}}} \tag{7}$$

in which σ_{cf} is the static uniaxial compression yield stress with the lowest strain rate and $\bar{\sigma}_{\mathrm{cf}}$ is the yield stress at a nonzero strain rate.

3.2 Modelling of CFRP materials

The numerical and experimental results were compared for the validation of the numerical method. Fig. 7 shows the nominal stress versus nominal strain curves of the core with l_{w} = 10 mm and ρ_{f} = 75 kg/m^3, obtained from the compression test and numerical simulation, respectively, while Fig. 8 shows the comparison of the deformation of the core at a certain nominal strain (ε_{n} = 0.15).

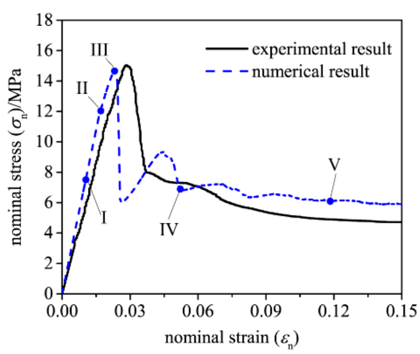

Fig. 7 Comparison of nominal stress versus nominal strain curves of the core with l_{w} = 10 mm, h_{c} = 20 mm and ρ_{f} = 75 kg/m^3 between experimental and numerical results

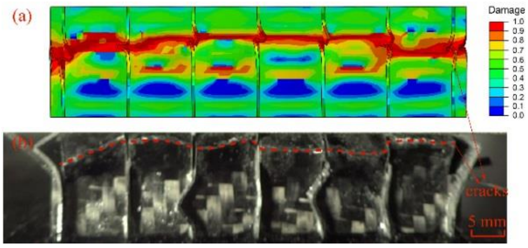

Fig. 8 Comparison of the failure mode of the core at the nominal strain of $\varepsilon_n = 0.15$ between experiments and numerical simulations

It can be seen from Fig. 8 that the numerical model can accurately predict the failure mode of the core, including the cracks and the folding of the honeycomb walls. We can see from Fig. 7 that the compressive stress of the core increases linearly first and then drops to a plateau state after the failure of the honeycomb. In the tested specimen, there were uncertain imperfections in the adhesive bounding between the honeycomb and foam fillers, which cannot be considered in the numerical model. Consequently, the stress in plateau state from the numerical simulation was larger than that from the test because the failure of the bonding cannot be considered in this numerical model. Overall, the numerical and experimental results agree well, which provides that the numerical model is validate enough to predict the quasi static compressive response of the core.

4. Results and discussion

4.1 Compressive deformation and energy absorption process of the core

Taking the l_w = 10 mm and h_c = 20 mm CFRP honeycomb with foam fillers of density ρ_f = 75 kg/m^3 for instance, the quasi static compressive deformation process of the core is described by Figs. 7 and 9.

As shown in Fig. 7, the deformation process of the core while $\varepsilon_n \le 0.15$ can be divided into four stages, i.e. the linear elastic stage ($0 < \varepsilon_n < 0.016$), the honeycomb wall buckling stage ($0.016 \le \varepsilon_n < 0.026$), the honeycomb failure stage ($0.026 \le \varepsilon_n < 0.046$) and the plateau stage ($\varepsilon_n \ge 0.046$). During the first stage, as shown in Fig. 9(a), the core is uniformly compressed in the thickness direction. The core gives a linear elastic response and thus no damage occurs. With the strain increases, the CFRP honeycomb buckles at the nominal strain of $\varepsilon_n = 0.016$, which can be seen in Fig. 9(b) and the increasing rate of the stress decreases accordingly. Then the stress reaches its peak value at the nominal strain of $\varepsilon_n = 0.026$ and at this point the failure of the honeycomb initiates; it can be seen from Fig. 9(c) that the damage variable reaches to the value of 1 and bending deformation occurs in honeycomb walls. After that the honeycomb collapses and the stress drops to a nearly plateau value and with the compressive process continues, cracks appear in damage areas and folding of the honeycomb walls can be observed in Figs. 9(d) and (e).

We proceed to analyze the energy absorption process of the core during the compression. Define the energy absorbed by the core with E_a and it can be derived by

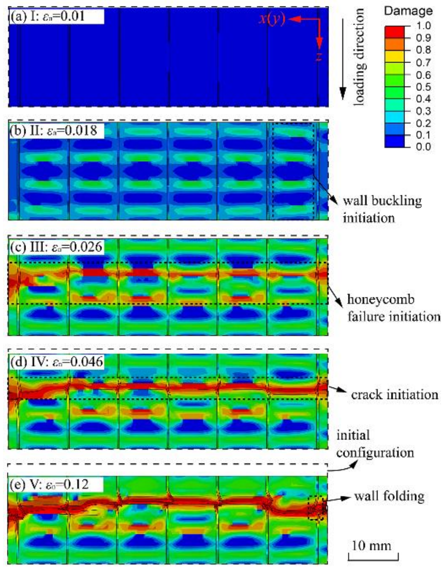

Fig. 9 Compressive deformation process of the core with l_w = 10 mm, h_c = 20 mm, and ρ_f = 75 kg/m^3

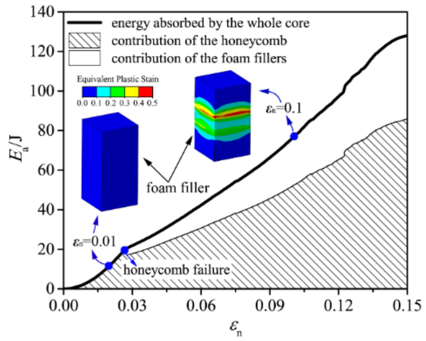

Fig. 10 Energy absorption process of the core with l_w = 10 mm, h_c = 20 mm and ρ_f = 75 kg/m^3

$$E_a = \int_0^s F ds \tag{8}$$

where s is the compressive displacement and F is the compressive force.

Fig. 10 shows the energy absorption process of the core with l_w = 10 mm, h_c = 20 mm and ρ_f = 75 kg/m^3, including the contribution of the CFRP honeycomb and foam fillers and the deformation of the foam filler shown by equivalent plastic strain (PEEQ) at two specific nominal strain. It can be seen that before the initiation of the honeycomb failure, the energy absorption of the core is dominated by the honeycomb. It is because that during this stage, the deformation of the foam fillers is negligible and no plastic damage occurs. Then after the honeycomb fails, the foam fillers deform gradually under effects of the compressive loading and the deformation of the honeycomb. Consequently, energy absorbed by the foam fillers increases with the increase of the nominal strain and the contribution of the foam fillers on energy absorption is also increasing. Overall, the energy absorbed by foam fillers is fewer than that by the honeycomb. When ε_n = 0.15, the energy absorbed by the foam fillers is about 33.3% of the total energy absorbed by the core, while the contribution of the honeycomb on the energy absorption is about 66.7%.

4.2 Effects of the core height on the compressive properties

In order to analyze the effects of the core height on the compressive response of this hybrid core structure, we simulated the compression of the hybrid cores with fixed spacing between honeycomb walls (l_w = 10 mm) and foam density (ρ_f = 75 kg/m^3), and different core heights. The compressive nominal stress versus nominal strain curves of the hybrid cores, of which the core height is h_c = 10 mm, 20 mm, 30 mm, and 40 mm, respectively, are shown in Fig. 11.

We can see from Fig. 11 that the core height has no effect on the linear elastic response and buckling initiation of the hybrid core. Nevertheless, the peak stress and the plateau stress of the core change along with the core height. Specifically, with the increase of the core height, the peak stress decreases while the plateau stress increases. As mentioned before, for the configuration of the core used in this paper, the peak stress of the core is dominated by the buckling failure of the honeycomb. The decrease of the peak stress is due to the reduce of the stability of the core with the increase of the core height. So the honeycomb walls are more likely to buckle with a higher configuration, which can lead to earlier initiation of core buckling failure. The increase of the plateau stress is because that the compressive displacement increases with the increase of core height at the same nominal strain. Thus, the stress level in the foam fillers increases and consequently the plateau stress increases as well.

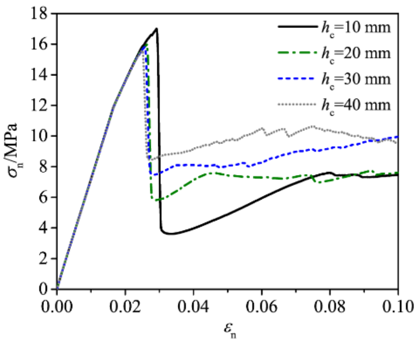

Fig. 11 Nominal stress versus nominal strain curves of hybrid cores with different core height (l_w = 10 mm, ρ_f = 75 kg/m^3)

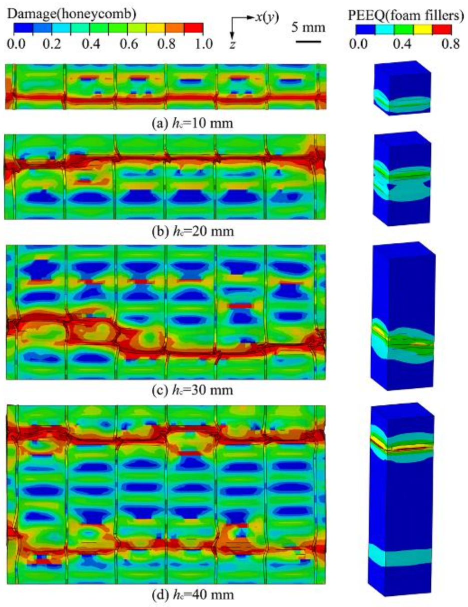

Fig. 12 Comparison of the compressive deformation of hybrid cores with different core height when ε_n = 0.1

Fig. 12 shows the deformation of hybrid cores with different heights at the nominal strain of ε_n = 0.1. It can be seen that with the increase of the core height, the compressive displacement increases and the bending and folding of the honeycomb walls become more severe. When the core height reaches to h_c = 40 mm, two main cracks appear in the honeycomb while there is only one crack in cores with smaller height. The plastic deformation of the foam fillers also becomes more severe with the increase of the core height.

Table 3 gives the comparison of the peak stress and energy absorption properties between hybrid cores with different heights, in which σ_p is the peak stress of the core during compression, E_a is the energy absorbed the whole core, E_h is the energy absorbed by the honeycomb, E_f is the energy absorbed by the foam fillers, m is the total mass of the core, E_s is the specific energy of the core that can be calculated by $E_s = E_a/m$, Δm and ΔE_s is the change of the core mass and specific energy, respectively.

We can see from Table 3 that the peak stress decreases slightly with the increase of the core height, while the absorbed energy increases dramatically due to the more severe deformation of the core with larger core height. The specific energy absorption also increases with core height increasing. Comparing the contribution of the honeycomb and foam fillers on the energy absorption, it can be seen that with different core heights, the honeycomb always absorbs more energy than foam fillers, and the ratio of the energy absorbed by the honeycomb to that by foam fillers is about 2.1~2.5.

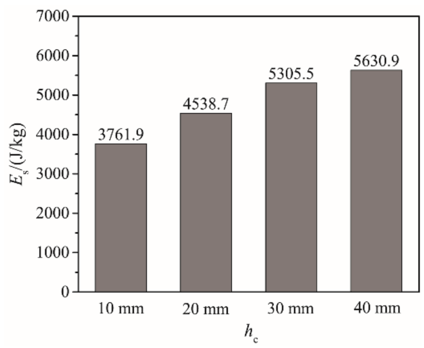

Fig. 13 Bar chart of the specific energy absorption of the hybrid cores with different core height when ε_n = 0.1

Table 3 Effects of the core height (h_c) on the compressive strength and energy absorption of the hybrid core (ε_n = 0.1)

h_c/mm	σ_p/MPa	E_a/J	E_h/J	E_f/J	m/g	Δm/%	E_s/(J/kg)	ΔE_s/%
10	17.0	31.6	22.5	9.1	8.4	-	3761.9	-
20	16.1	76.4	52.3	24.1	16.8	+100	4538.7	+20.6
30	15.8	133.7	89.1	44.6	25.2	+200	5305.5	+41.0
40	15.6	189.2	130.3	58.9	33.6	+300	5630.9	+49.7

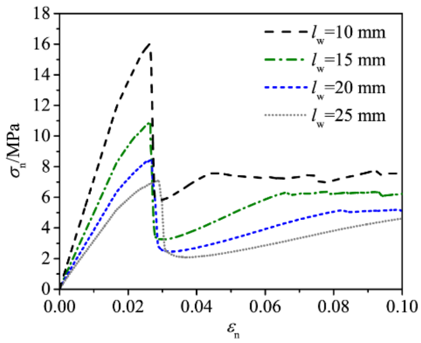

Fig. 14 Nominal stress versus nominal strain curves of hybrid cores with different spacing between honeycomb walls (h_c = 20 mm, ρ_f = 75kg/m^3)

As can be seen from Fig. 13, with the core height increases from 10 mm to 40 mm, the specific energy absorption increases by 20.6%, 41.0% and 49.7%, respectively. However, noting that the core mass increases linearly with the increase of the core height (100%, 200% and 300% increase for h_c = 20 mm, 30 mm and 40 mm, respectively), the effects of the mass increase should be considered when trying to improve the energy absorption properties by increasing the core height.

4.3 Effects of the spacing between honeycomb walls on the compressive properties

Keep the core height h_c = 20 mm and foam density ρ_f = 75 kg/m^3 fixed, effects of the spacing between honeycomb walls (l_w) on the compressive properties of the core were analyzed. The compressive stress versus strain relations of the hybrid core with different l_w was shown in Fig. 14. It can be seen that with the increase of l_w, the elastic compressive modulus, the peak stress as well as the plateau stress of the core are all decreased, which means that the increase of l_w makes the core weaker.

Fig. 15 shows the deformation of the hybrid core with different l_w when ε_n = 0.1. It can be seen from Fig. 14 that the deformation of the honeycomb and the foam fillers are both more severe when l_w is smaller. Specifically, when l_w = 10 mm, folding deformation occurred in the honeycomb and the fracture of the honeycomb and the deformation of the foam fillers are more severe. As l_w increased, the damage of the honeycomb becomes less severe. The deformation of honeycomb walls gradually turns into overall bending from folding.

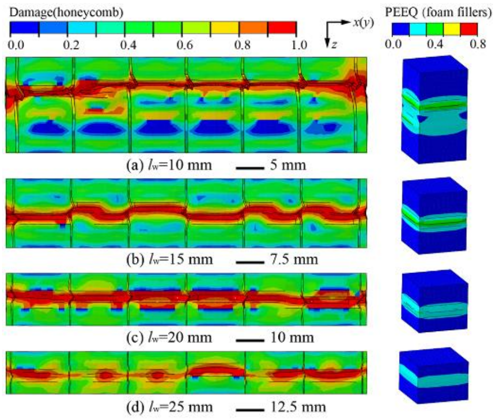

Fig. 15 Comparison of the compressive deformation of the hybrid cores with different spacing between honeycomb walls when ε_n = 0.1

Table 4 shows the effects of l_w on the compressive strength and energy absorption of the hybrid cores. We can also see that the peak stress of the core decreases notably with the increase of l_w (Fig. 16). Besides, the absorbed energy increases with the increase of l_w. However, due to the increase of the mass, the specific energy absorption presents a decreasing trend with the increase of l_w, which shows that the hybrid core is more energy absorption efficient with a smaller spacing between honeycomb walls.

In addition, the contribution of the honeycomb on the energy absorption decreases from 68.4% to 55.5% with l_w increases from 10 mm to 25 mm; the contribution of foam fillers increases from 32.6% to 44.5% accordingly.

Table 4 Effects of the spacing between walls (l_w) on the compressive strength and energy absorption of the hybrid core (ε_n = 0.1)

l_w/mm	σ_p/MPa	E_a/J	E_h/J	E_f/J	m/g	Δm/%	E_s/(J/kg)	ΔE_s/%
10	16.1	76.4	52.3	24.1	16.8	-	4538.7	-
15	10.9	105.8	60.7	45.1	35.4	+110.7	2988.7	-34.2
20	8.4	134.6	74.5	60.1	50.2	+198.8	2681.3	-40.9
25	7.1	168.9	93.8	75.1	67.7	+303.0	2494.8	-45.0

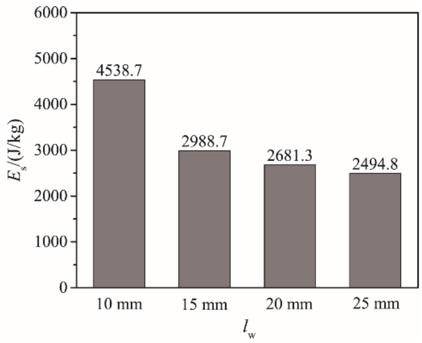

Fig. 16 Bar chart of the specific energy absorption of the hybrid cores with different spacing between honeycomb walls when $\varepsilon_n = 0.1$

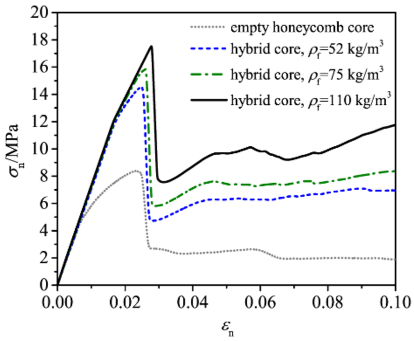

Fig. 17 Nominal stress versus nominal strain curves of empty honeycomb and honeycombs with foam fillers of different densities ($l_w = 10$ mm, $h_c = 20$ mm)

4.4 Effects of the PMI foam fillers on the compressive properties

Effects of foam fillers on the compressive properties of the CFRP honeycomb was analyzed. Simulations of the compression of empty honeycomb and honeycombs with PMI foam fillers of which the densities are 52 kg/m^3, 75 kg/m^3 and 110 kg/m^3 were conducted, respectively. Fig. 17 shows the compressive stress versus strain curves of different cores, from which we can see that the foam fillers have a significant effect on the peak stress and plateau stress of the core. Specifically, the foam fillers can improve the stability of the honeycomb, therefore the buckling failure of the honeycomb walls occurs at a larger nominal strain and the peak stress increased accordingly. Additionally, with the increase of the foam density, the peak stress and the plateau stress increases at the same time, which shows that foam fillers with larger density have better reinforcing effect on the compressive strength of the honeycomb.

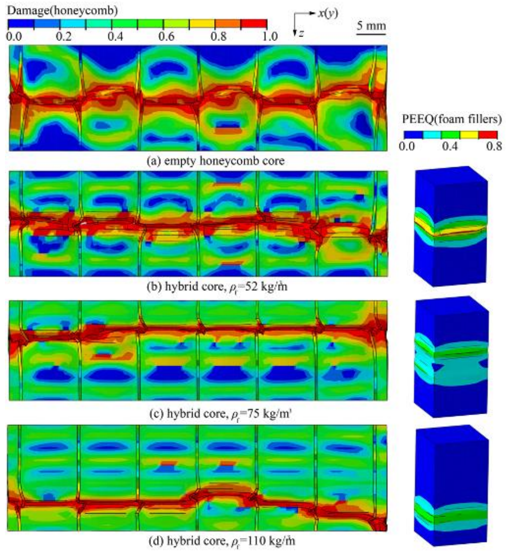

Fig. 18 Comparison of the compressive deformation of empty honeycomb and honeycombs with foam fillers of different densities when $\varepsilon_n = 0.1$

Fig. 18 shows the deformation of the empty honeycomb core and hybrid core with different foam fillers when ε_n = 0.1. It can be seen that there is no obvious change in the failure mode of the honeycomb after filled with foam fillers, cracks and wall folding can be found in all the four cases. Due to the worse stability, the bending deflection of empty honeycomb walls is more severe; the bending deflection of the honeycomb walls with foam fillers and the plastic deformation of foam fillers decreases with the increase of the foam density. From Fig. 16 we can also see that the fracture failure of core became more localized with foam fillers and the localization becomes more obvious with the increase of the foam density.

Table 5 contains the comparison of the peak stress and energy absorption properties of the empty and hybrid cores with different foam fillers. It shows that the foam fillers markedly increase the strength and the energy absorbing capacity of the honeycomb.

Furthermore, comparison of the specific energy absorption shows that the foam fillers also improve the energy absorption efficiency of the honeycomb (Fig. 19). Compared to the empty honeycomb, with foam fillers of densities ρ_f = 52 kg/m^3, 75 kg/m^3 and 110 kg/m^3, the specific energy absorbed by the core increases by 70.0%, 80.2% and 92.2%, respectively, while the mass of the core increases by only 33.3%, 47.4% and 70.2%, respectively.

Table 5 Effects of the foam fillers on the compressive strength and energy absorption of the core ($\varepsilon_n = 0.1$)

Core type	σ_p/MPa	E_a/J	E_h/J	E_f/J	m/g	Δm/%	E_s/(J/kg)	ΔE_s/%
Honeycomb	8.4	28.8	28.8	-	11.4	-	2519.0	-
Hybrid, ρ_f = 52 kg/m^3	14.6	65.0	45.2	19.8	15.2	+33.3	4282.7	+70.0
Hybrid, ρ_f = 75 kg/m^3	16.1	76.4	52.3	24.1	16.8	+47.4	4538.7	+80.2
Hybrid, ρ_f = 110 kg/m^3	17.8	93.7	57.0	36.7	19.4	+70.2	4841.6	+92.2

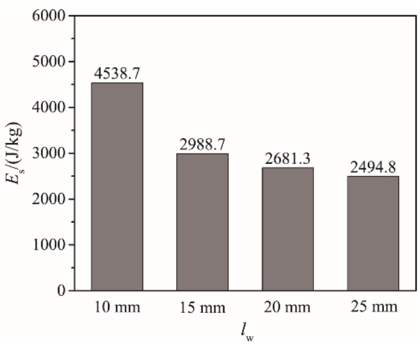

Fig. 19 Bar chart of the specific energy absorption of empty honeycomb and honeycombs with foam fillers of different densities when $\varepsilon_n = 0.1$

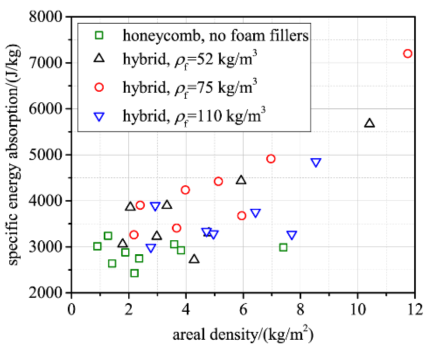

Fig. 21 Specific energy absorption of honeycombs with and without foam fillers

4.5 Comparison of compressive properties between square CFRP honeycombs with and without foam fillers

In order to furtherly analyze the compressive properties of the square CFRP honeycomb reinforced by PMI foam fillers, the compressive strength and specific energy absorption of cores with different densities were presented and the compressive properties of empty honeycombs and honeycombs reinforced by PMI foam fillers with different densities were compared. The range of the spacing between honeycomb walls is from 10 mm to 30 mm while the range of the core height is from 15 mm to 60 mm.

Fig. 20 shows the comparison of the compressive strength versus density between different cores. We can see from Fig. 20 that for all the four types of cores, the compressive strength increases in a nearly linear mode with the increase of the core density. The increasing rate of the compressive strength of the honeycomb with foam fillers is higher than that of the empty honeycomb. Furthermore, it can be seen that with the same configuration, the density and compressive strength of the empty honeycomb are both in a lower level compared with honeycomb with foam fillers. As for the honeycomb with foam fillers, the compressive strength of the core decreases with the increase of the foam density when the density of the core is the same. It shows that the effects of the increase of foam density on the increase of the compressive strength is not significant compared with its effects on the increase of the core mass.

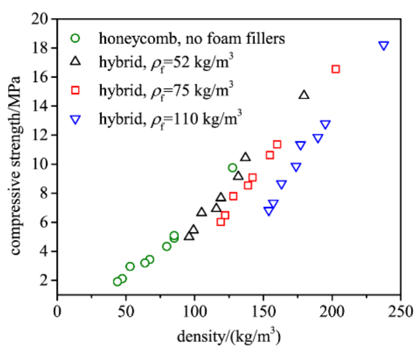

Fig. 20 Compressive strength of honeycombs with and without PMI foam fillers

As discussed above, the core height has a significant influence on the energy absorption of the core. Consequently, in order to compare the energy absorption properties of different cores, we use areal density to distinguish cores with different configurations because the areal density is a parameter which can take the core height into account while the density cannot. The comparison of the specific energy absorption versus areal density between different cores is shown in Fig. 21.

It can be seen that compared with honeycomb with foam fillers, the specific energy absorption of the empty honeycomb remains in a lower level of about 3000 J/kg and there is no obvious change in specific energy absorption with varying areal density. As for the honeycomb with foam fillers, the specific energy absorption presents a slight overall increasing trend with the increase of the areal density. Comparing the energy absorption properties of the honeycomb with different foam fillers, it can be seen that honeycombs with foam fillers of density ρ_f = 52 kg/m^3 and 75 kg/m^3 are more energy efficient than honeycombs with foam fillers of ρ_f = 110 kg/m^3.

5. Conclusions

A hybrid core with thin-walled square CFRP honeycomb and PMI foam fillers was proposed and fabricated. The quasi static compressive properties of the core were analyzed by numerical simulations. Main conclusions are as follows:

- With the increase of the core height, the compressive strength of the core slightly drops while the specific energy absorbed by the core increases. The damage of the core becomes more severe with the increase of the core height.
- With the increase of the spacing between honeycomb walls, the compressive strength of the core decreases dramatically and the specific energy absorbed by the core decreases as well.
- The PMI foam fillers can significantly improve the compressive properties of the CFRP honeycomb by increasing the compressive strength and specific energy absorption. With the increase of the foam density, the compressive strength and specific energy

absorption of the core both present an increasing trend.

Acknowledgments

We are grateful for access to the universe testing machine of Prof. Xianfeng Zhang's group in Nanjing University of Science and Technology.

References

Aydin, M.R. and Gundogdu, O. (2018), "Vibration analysis of honeycomb sandwich composites filled with polyurethane foam by Taguchi Method", *Steel Compos. Struct., Int. J.*, **28**(4), 461-470. https://doi.org/10.12989/scs.2018.28.4.461

Deshpande, V.S. and Fleck, N.A. (2001), "Multi-axial yield behaviour of polymer foams", *Acta Mater*., **49**, 1859-1866. https://doi.org/10.1016/s1359-6454(01)00058-1

Fan, H.L., Meng, F.H. and Yang, W. (2006), "Mechanical behaviors and bending effects of carbon fiber reinforced lattice materials", *Arch. Appl. Mech.*, **75**, 635-647. https://doi.org/10.1007/s00419-006-0032-x

George, T., Deshpande, V.S., Sharp, K. and Wadley, H.N.G. (2014), "Hybrid core carbon fiber composite sandwich panels: fabrication and mechanical response", *Compos. Struct.*, **108**, 696-710. https://doi.org/10.1016/j.compstruct.2013.10.002

Hu, Y., Li, W., An, X. and Fan, H. (2016), "Fabrication and mechanical behaviors of corrugated lattice truss composite sandwich panels", *Compos. Sci. Technol.*, **125**, 114-122. https://doi.org/10.1016/j.compscitech.2016.02.003

Hussein, R.D., Ruan, D., Lu, G.X., Guillow, S. and Yoon, J.W. (2017), "Crushing response of square aluminium tubes filled with polyurethane foam and aluminium honeycomb", *Thin-Wall. Struct.*, **110**, 140-154. https://doi.org/10.1016/j.tws.2016.10.023

Liu, Q., Fu, J., Wang, J., Ma, J., Chen, H., Li, Q. and Hui, D. (2017), "Axial and lateral crushing responses of aluminum honeycombs filled with EPP foam", *Compos. Pt. B-Eng.*, **130**, 236-247. https://doi.org/10.1016/j.compositesb.2017.07.041

Mozafari, H., Crupi, V., Epasto, G. and Guglielmino, E. (2015), "In plane compressive response and crushing of foam filled aluminum honeycombs", *J. Compos Mater.*, **49**, 3215-3228. https://doi.org/10.1177/0021998314561069

Norouzi, H. and Rostamiyan, Y. (2015), "Experimental and numerical study of flatwise compression behavior of carbon fiber composite sandwich panels with new lattice cores", *Constr. Build. Mater.*, **100**, 22-30. https://doi.org/10.1016/j.conbuildmat.2015.09.046

Reddy, T.Y. and Wall, R.J. (1988), "Axial compression of foam-filled thin-walled circular tubes", *Int. J. Impact Eng.*, **7**, 151-166. https://doi.org/10.1016/0734-743X(88)90023-1

Russell, B.P., Deshpande, V.S. and Wadley, H. (2008), "Quasistatic deformation and failure modes of composite square honeycombs", *J. Mech. Mater. Struct.*, **3**(7), 1315-1340. https://doi.org/10.2140/jomms.2008.3.1315

Seibert, H.F. (2000), "PMI foam cores find further applications", *Reinf Plast.*, **44**, 36-38. https://doi.org/10.1016/S0034-3617(00)86485-1

Taghipoor, H. and Noori, M.D. (2018a), "Experimental and numerical study on energy absorption of lattice-core sandwich beam", *Steel Compos. Struct., Int. J.*, **27**(2), 135-147. https://doi.org/10.12989/scs.2018.27.2.135

Taghipoor, H. and Noori, M.D. (2018b), "Experimental and numerical investigation of lattice core sandwich beams under low-velocity bending impact", *J. Sandw. Struct. Mater.*, **21**(6), 2154-2177. https://doi.org/10.1177/1099636218761315

Taghipoor, H. and Noori, M.D. (2018c), "Axial crushing and transverse bending responses of sandwich structures with lattice core", *J. Sandw. Struct. Mater*. https://doi.org/10.1177/1099636218761321

Zhang, Y., Liu, Q., He, Z., Zong, Z. and Fang, J. (2019), "Dynamic impact response of aluminum honeycombs filled with expanded polypropylene foam", *Compos. Pt. B-Eng.*, **156**, 17-27. https://doi.org/10.1016/j.compositesb.2018.08.043.

CC

Appendix: Details of the damage law of CFRP mateials

The material is taken to be linear elastic up to the initiation of damage and a nonlinear stress versus strain response accompanies damage progression due to a progressive drop in the elastic moduli with the increasing strain. Four scalar damage variables di are introduced, corresponding to four damage modes (tensile and compressive failure in each of the fiber and transverse directions). In the undamaged state each damage variable is set to zero. Rate controlled damage accumulates with strain and the moduli drop with the increase of damage variables, so that one or more moduli equal to zero when one of the damage variables attains unity.

The tensile and compressive strengths for damage initiation in the undamaged material in the fiber direction (x_1 direction) are denoted by X^{T} and X^{C}, respectively. The corresponding tensile and compressive strengths in the transverse direction are denoted by Y. Strengths begin to drop after damage has developed. Write the damage variable for tensile failure in the fiber direction as d_f^t and thus the current tensile strength in the fiber direction is$\left(1-d_f^t\right)X^T$. Similarly, damage variables for compressive failure in the fiber direction is d_f^c, while that for transverse tension and compression is d_m^t and d_m^c, respectively. The scalar damage d_s is defined as

$$d_s \equiv 1-\left(1-d_f^t\right)\left(1-d_f^c\right)\left(1-d_m^t\right)\left(1-d_m^c\right) \tag{9}$$

In any given state of damage, the secant relationship between stress and strain reads

$$\begin{pmatrix}\varepsilon_{11}\\ \varepsilon_{22}\\ \gamma_{12}\end{pmatrix}=\begin{pmatrix}\dfrac{1}{\left[E_1\left(1-d_f\right)\right]} & -\nu_{21}\left[E_1\left(1-d_f\right)(1-d_m)\right] & 0\\ -\nu_{12}\left[E_2(1-d_m)\left(1-d_f\right)\right] & \dfrac{1}{\left[E_2(1-d_m)\right]} & 0\\ 0 & 0 & \dfrac{1}{G(1-d_s)}\end{pmatrix}\begin{pmatrix}\sigma_{11}\\ \sigma_{22}\\ \sigma_{12}\end{pmatrix} \tag{10}$$

where

$$d_f=\begin{cases}d_f^t & \text{if } \sigma_{11}\geq 0\\ d_f^c & \text{if } \sigma_{11}<0\end{cases} \tag{11}$$

and

$$d_m=\begin{cases}d_m^t & \text{if } \sigma_{22}\geq 0\\ d_m^c & \text{if } \sigma_{22}<0\end{cases} \tag{12}$$

Assuming that the stress decreases linearly with the increase of the strain once damage initiates. The damage evolution law for each of the four damage variables d_f^t, d_f^c, d_m^t and d_m^c, with the corresponding rate-dependent reference values denoted by D_f^t, D_f^c, D_m^t and D_m^c, respectively, are described as follows. Taking the fiber tensile damage mode for instance, an effective strain is defined as $\hat{\varepsilon}_f^t = \langle \varepsilon_{11} \rangle$ and it is used to update the damage state variable via the relation

$$D_f^t = \frac{\frac{2E_f^t}{L_e X^T}\left(\hat{\varepsilon}_f^t - \frac{X^T}{E_1}\right)}{\hat{\varepsilon}_f^t\left(\frac{2E_f^t}{L_e X^T} - \frac{X^T}{E_1}\right)} \le 1 \tag{13}$$

where E_f^t is the fracture energy for fiber compression failure and the effective strain is $\hat{\varepsilon}_f^c = \langle -\varepsilon_{11} \rangle$.

The matrix damage variables are given by

$$D_m^t = \frac{\frac{2E_m}{L_e Y}\left(\hat{\varepsilon}_m^t - \frac{Y}{E_2}\right)}{\hat{\varepsilon}_m^t\left(\frac{2E_m}{L_e Y} - \frac{Y}{E_2}\right)} \le 1 \tag{14}$$

and

$$D_m^c = \frac{\frac{2E_m}{L_e Y}\left(\hat{\varepsilon}_m^c - \frac{Y}{E_2}\right)}{\hat{\varepsilon}_m^c\left(\frac{2E_m}{L_e Y} - \frac{Y}{E_2}\right)} \le 1 \tag{15}$$

where J_m is the matrix fracture energy and the effective stain for matrix tension and compression are defined as $\hat{\varepsilon}_m^t = \sqrt{\langle \varepsilon_{22} \rangle^2 + \varepsilon_{12}^2}$ and $\hat{\varepsilon}_m^c = \sqrt{\langle -\varepsilon_{22} \rangle^2 + \varepsilon_{12}^2}$, respectively.

Finally, the current value of each of the damage variables is specified via a rate law. The damage variables can be specified as the solution to the first order differential equation

$$\dot{d} = \frac{1}{\tau}(D - d) \tag{16}$$

where τ is a time constant that governs the rate at which d attains its steady state value D.

In this paper, the parameters of CFRP material in the numerical model were obtain from quasi static test on CFRP sheets based on standards of GB/T 1445-2005 and GB/T 3354-2014. The broken of the tensile specimen are shown in Fig. A1.

Details of the parameters are given in Table A1.

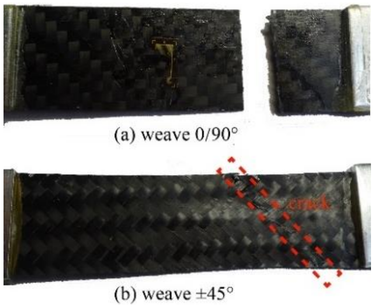

Fig. A1 Broken of the CFRP specimen in the tensile test: (a) tensile in 0/90° fiber direction; and (b) tensile in ±45° fiber direction

Table A1 The materials properties of water each unidirectional ply of the woven CFRP materials employed in the constitutive model in the calculations

Material	Property	Value
	E_1	9.6 GPa
	E_2	4.5 GPa
	G	3.5 GPa
	υ_{12}	0.16
	X^T	390 MPa
	X^C	382 MPa
Woven	Y	76 MPa
	E_f^t/L_e	9.5 MPa
	E_f^c/L_e	9.1 MPa
	E_m/L_e	11.4 MPa
	ply thickness	0.2 mm
	ρ_c	1450 kg/m^3
	τ	8 μs